POLSAR Image Analysis of Wetlands Using a Modified Four-Component Scattering Power Decomposition

Yuki Yajima, Yoshio Yamaguchi, *Fellow, IEEE*, Ryoichi Sato, *Member, IEEE*, Hiroyoshi Yamada, *Member, IEEE*, and Wolfgang-Martin Boerner, *Life Fellow, IEEE*

***Abstract*—It is important to monitor environmental changes of the Earth's cover by remotely sensed data. This paper analyzes seasonal changes of a wetland by a modified polarimetric four-component scattering power decomposition method. The data sets analyzed here are L- and X-band fully polarimetric synthetic aperture radar (POLSAR) data, which have been acquired by the NICT/JAXA airborne polarimetric and interferometric synthetic aperture radar system in 2004. Since there existed a deficiency in the currently adopted decomposition schemes in that negative powers appear in a few pixels in the image analysis, we modified the approach taking into account physical conditions. It is shown by the modified scheme that the seasonal changes and features of the vegetation near Sakata Lagoon in Niigata, Japan, are observed clearly, demonstrating the utility of POLSAR image analysis for wetland assessments in general.**

***Index Terms*—Coherency matrix, polarimetric synthetic aperture radar (POLSAR), radar polarimetry, scattering contribution decomposition, wetland assessment.**

I. Introduction

LAND cover monitoring is one of the most important applications of polarimetric synthetic aperture radar (POLSAR) sensing. Decomposition of polarimetric scattering matrices acquired by the POLSAR imaging system can provide the contribution of scattering mechanisms and extract environmental changes by comparing data sets of consecutive seasonal observations. Based on second-order statistics of the scattering matrix, various decomposition techniques have been proposed [1]–[5]. We focus our attention at the scattering power decomposition methods, which deal with the reflection symmetric case $\langle S_{HH}S_{HV}^{*}\rangle \approx \langle S_{VV}S_{HV}^{*}\rangle \approx 0$ [1], and the nonreflection symmetric case $\langle S_{HH}S_{HV}^{*}\rangle \neq 0$ and $\langle S_{VV}S_{HV}^{*}\rangle \neq 0$ [2]. The scheme based on the coherency matrix approach [2] has advantages such that the decomposed power can be expressed in terms of scattering elements directly, which is suitable for direct physical interpretation of data as related to pertinent scattering phenomena and for uncomplicated computation and easy implementation.

However, there exists a deficiency in implementation in that some negative powers appear in the image analysis. This negative power is inconsistent with physical conditions. Although the occurrence is rare and the magnitude is small, it increases in area containing man-made structures (nonreflection symmetric case). If the corrections are made in area with man-made structures, the modified algorithm should be applicable to all areas with general scattering case. Therefore, the purpose of this paper is to modify the decomposition procedure so that all the powers are positive physical constraints. Then we show the decomposition results applied to monitoring seasonal changes of a wetland area using high-resolution POLSAR data. The site is located at 37°49′N 138°53′E in Niigata Prefecture, Japan, where Sakata Lagoon has been registered as a Ramsar site (one of 33 sites in Japan) according to the Convention on Wetlands of International Importance, particularly the Migratory Waterfowl Habitat (Ramsar Treaty [6]).

In Section II, a brief summary of the four-component decomposition scheme is provided, and a modification of the decomposition approach is explained from a physical point of view in Section III. The modified scheme is applied to polarimetric-interferometric (Pi) SAR data sets in Section IV. Seasonal vegetation changes of the site are shown in Section V.

II. Four-Component Decomposition by Coherency Matrix

The ensemble average of the coherency matrix is given as

$$\langle [T] \rangle = \langle \boldsymbol{k}_P \boldsymbol{k}_P^{\dagger} \rangle \tag{1}$$

where † denotes complex conjugation and transposition, and the Pauli vector $\boldsymbol{k}_P$ is defined as

$$\boldsymbol{k}_P = \frac{1}{\sqrt{2}} \begin{bmatrix} S_{HH} + S_{VV} \\ S_{HH} - S_{VV} \\ 2S_{HV} \end{bmatrix}. \tag{2}$$

We expand the measured coherency matrix into four sub matrices as

$$\langle [T] \rangle = f_s [T]_{surface} + f_d [T]_{double} + f_v \langle [t] \rangle_{vol} + f_c \langle [T] \rangle_{helix} \tag{3}$$

Manuscript received March 11, 2007; revised September 16, 2007. This work was supported in part by a Grant in Aid for Scientific Research, the Japan Society for the Promotion of Science.

Y. Yajima, Y. Yamaguchi, and H. Yamada are with the Faculty of Engineering, Niigata University, Niigata 950-2181, Japan (e-mail: yamaguch@ie.niigata-u.ac.jp).

R. Sato is with the Faculty of Education, Niigata University, Niigata 950-2181, Japan.

W.-M. Boerner is with the University of Illinois at Chicago, Chicago, IL 60607 USA.

Color versions of one or more of the figures in this paper are available online at http://ieeexplore.ieee.org.

Digital Object Identifier 10.1109/TGRS.2008.916326

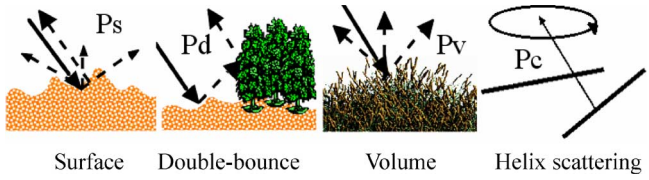

Fig. 1. Four-component scattering model.

where f_s, f_d, f_v, and f_c are the expansion coefficients to be determined. The expansion matrices are based on the scattering mechanisms, shown in Fig. 1, and can be constructed as follows [2]:

The surface scattering model

$$[T]_{surface} = \begin{bmatrix} 1 & \beta^* & 0 \\ \beta & |\beta|^2 & 0 \\ 0 & 0 & 0 \end{bmatrix}, \qquad |\beta| < 1 \tag{4}$$

and the double-bounce scattering model

$$[T]_{double} = \begin{bmatrix} |\alpha|^2 & \alpha & 0 \\ \alpha^* & 1 & 0 \\ 0 & 0 & 0 \end{bmatrix}, \qquad |\alpha| < 1 \tag{5}$$

where α and β are unknowns to be determined.

For the volume scattering model, we choose one of the following matrices according to the magnitude balance of $|S_{HH}|^2$ and $|S_{VV}|^2$.

- For $10\ \log(\langle|S_{VV}|^2\rangle/\langle|S_{HH}|^2\rangle) > 2$ dB

$$\langle[T]\rangle_{vol} = \frac{1}{30}\begin{bmatrix} 15 & -5 & 0 \\ -5 & 7 & 0 \\ 0 & 0 & 8 \end{bmatrix}. \tag{6}$$

- For $|10\ \log(\langle|S_{VV}|^2\rangle/\langle|S_{HH}|^2\rangle)| < 2$ dB

$$\langle[T]\rangle_{vol} = \frac{1}{4}\begin{bmatrix} 2 & 0 & 0 \\ 0 & 1 & 0 \\ 0 & 0 & 1 \end{bmatrix}. \tag{7}$$

- For $10\ \log(\langle|S_{VV}|^2\rangle/\langle|S_{HH}|^2\rangle) < -2$ dB

$$\langle[T]\rangle_{vol} = \frac{1}{30}\begin{bmatrix} 15 & 5 & 0 \\ 5 & 7 & 0 \\ 0 & 0 & 8 \end{bmatrix}. \tag{8}$$

The helix scattering model

$$\langle[T]\rangle_{helix} = \frac{1}{2}\begin{bmatrix} 0 & 0 & 0 \\ 0 & 1 & \pm j \\ 0 & \mp j & 1 \end{bmatrix}. \tag{9}$$

By comparing the measured data with the expansion matrices (3), we can obtain the corresponding scattering powers. Helix scattering power (circular polarization power): P_c

$$P_c = f_c = 2\left|\mathrm{Im}\left\langle S_{HV}^*(S_{HH} - S_{VV})\right\rangle\right|. \tag{10}$$

The volume scattering power: P_v for (7)

$$P_v = f_v = 8\langle|S_{HV}|^2\rangle - 2P_c. \tag{11}$$

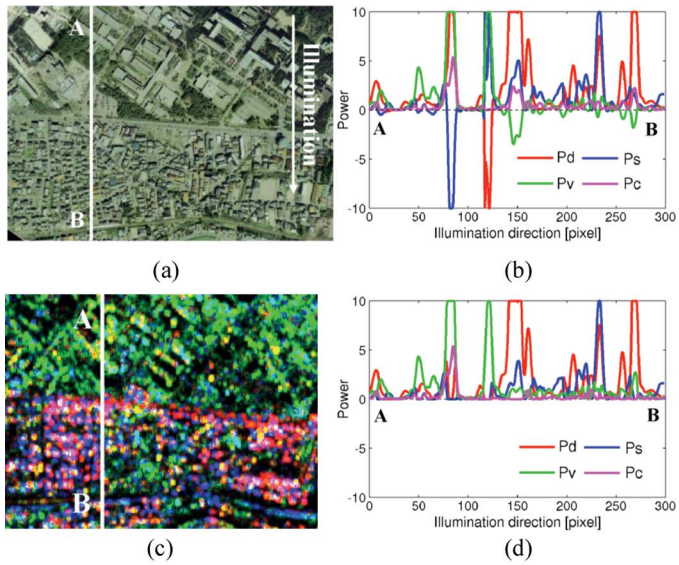

Fig. 2. Neighborhood of the Niigata University region and its polarimetric decomposition result: R (P_d), G (P_v), B (P_s), pink (P_c). (a) Aerial photo. (b) Power profile before modification. (c) Decomposed image. (d) Power profile after modification.

Because the number of unknowns exceeds the number of equations, we use another condition for determining the remaining powers: the surface scattering power P_s and the double-bounce scattering power P_d. Because the sign of $\mathrm{Re}\langle S_{HH}S_{VV}^*\rangle$ plays an important role for discriminating these two physically, we employ the additional criterion (see the Appendix)

$$C_0 = \langle S_{HH}S_{VV}^*\rangle - \langle|S_{HV}|^2\rangle + \frac{1}{2}P_c. \tag{12}$$

If $\mathrm{Re}\{C_0\} > 0$, then $\alpha = 0$, assuming the surface scattering is dominant

$$P_s = S + \frac{|C|^2}{S} \quad P_d = D - \frac{|C|^2}{S}. \tag{13a}$$

If $\mathrm{Re}\{C_0\} < 0$, then $\beta = 0$, assuming the double-bounce scattering is dominant

$$P_s = S - \frac{|C|^2}{D} \quad P_d = D + \frac{|C|^2}{D} \tag{13b}$$

where S, D, and C are given by

$$S = \frac{1}{2}\left\langle|S_{HH} + S_{VV}|^2\right\rangle - 4\left\langle|S_{HV}|^2\right\rangle + P_c \tag{14a}$$

$$D = \frac{1}{2}\left\langle|S_{HH} - S_{VV}|^2\right\rangle - 2\left\langle|S_{HV}|^2\right\rangle \tag{14b}$$

$$C = \frac{1}{2}\left\langle(S_{HH} + S_{VV})\,(S_{HH}^* - S_{VV}^*)\right\rangle. \tag{14c}$$

Finally, the four-component scattering powers P_s, P_d, P_v, and P_c are given by (10), (11), and (13), completing the four-component decomposition. The decomposition scheme yields the same results as would be obtained by the covariance matrix method provided in Yamaguchi *et al.* [3].

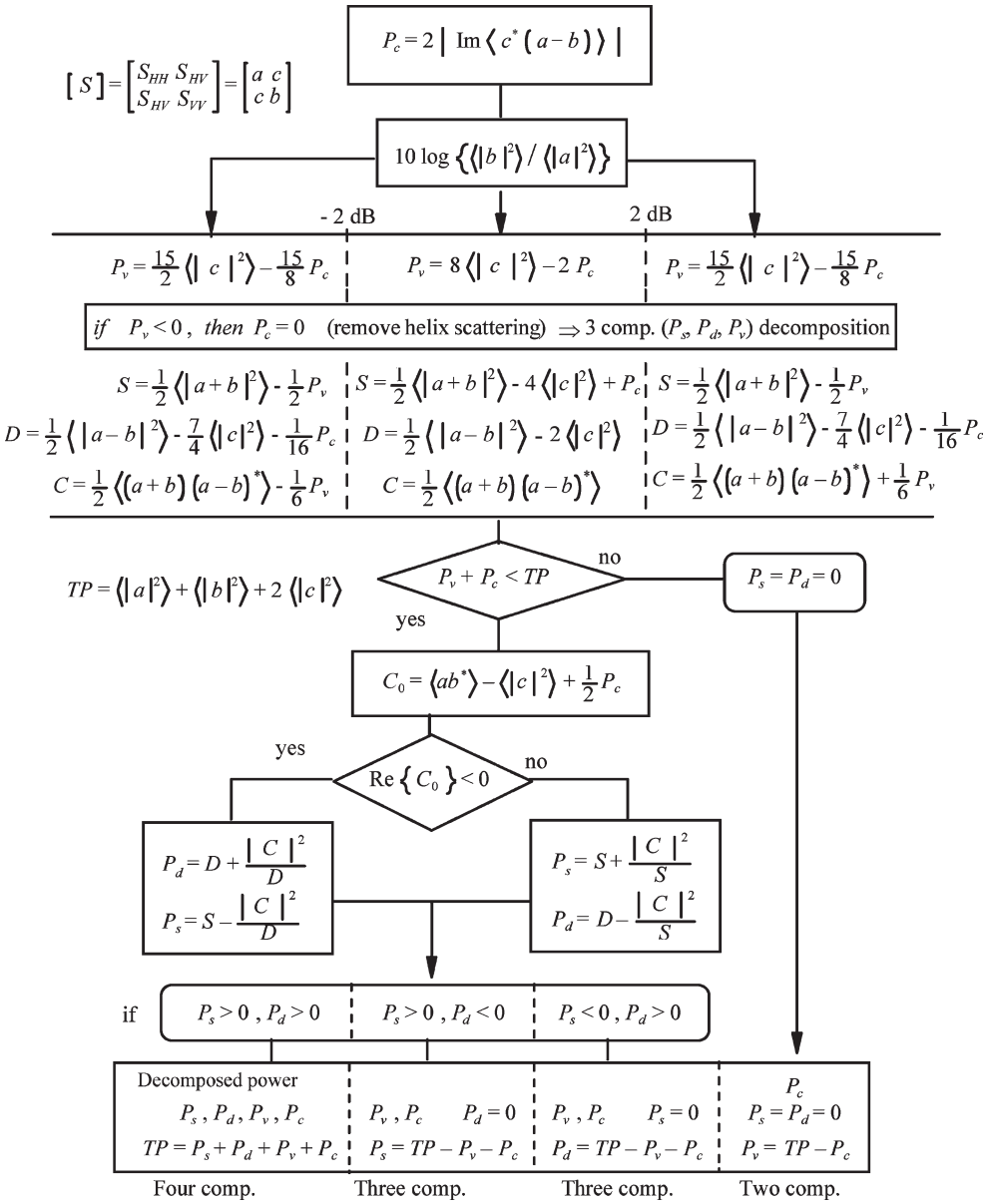

Fig. 3. Modified algorithm of four-component decomposition amended by power constraints.

III. Modification of the Decomposition Algorithm

A. Problem

We sometimes encounter a problem in high-resolution POLSAR image analysis in that negative powers occur in the data processing such that

1) $P_v < 0$;
2) $P_v + P_c >$ total power = TP [TP: the span of the coherency matrix (1)];
3) $P_s < 0$ or $P_d < 0$.

The reason for this discrepancy is deducible from the corresponding (11), (13), and (14). It is caused by relatively large values of $|S_{HV}|$ in the observed scattering matrices. Therefore, we checked some areas to see how often these adverse results occurred. The region chosen is in the neighborhood of Niigata University [Fig. 2(a)], which includes residential houses orthogonal to radar illuminations, pine trees, buildings nonorthogonal to radar illuminations, etc. This urban area exhibits the so-called nonreflection symmetry condition.

We calculated each power along a transect shown in Fig. 2(a), resulting in the power profiles along the transect in Fig. 2(b), where color-coded decomposed lines are illustrated with red (P_d), green (P_v), blue (P_s), and pink (P_c), respectively. We can see that some negative powers appear along the line. These are inconsistent with the physical phenomena.

B. Modification by Power Restriction

To overcome the inconsistency, a simple constraint on the scattered powers is applied such that all the powers should be positive and less than the total power.

1) $P_v < 0$: As we can see in (11), negative power is caused by the P_c being too large. We find these phenomena within

residential areas or at man-made structures because P_c is mainly caused by facets from man-made objects [3]. Actually, the scatterers with $P_v < 0$ in Fig. 2(b) were residential houses orthogonal to radar illumination, which are also accompanied with strong P_d. Because these scatterers with $P_v < 0$ exhibit large P_d, we assume that $P_c = 0$ if P_v becomes negative. The modification is if $P_v < 0$, then $P_c = 0$.

Enforcing $P_c = 0$ in this case might be against logic, but it is based on the ground truth data. This point may be further investigated considering tilted roof or slope scattering [7]. On the other hand, enforcing $P_c = 0$ for $P_v < 0$ leads to the three-component decomposition [1] automatically.

2) $P_v + P_c > TP$: Because P_v is proportional to $\langle |S_{HV}|^2 \rangle$, as seen in (11), the value sometimes exceeds the total power TP when $\langle |S_{HV}|^2 \rangle$ is relatively large

$$TP = \left\langle |S_{HH}|^2 + 2|S_{HV}|^2 + |S_{VV}|^2 \right\rangle .$$

For the areas exhibiting this characteristic, which include forest, crop fields, and oriented urban blocks, we can expect volume scattering to be dominant. Therefore, the modification becomes

$$\text{If } P_v > \text{TP}, \text{then } P_v = \text{TP}$$
$$\text{If } P_v + P_c > \text{TP}, \text{then } P_v = \text{TP} - P_c.$$

In this case, the surface scattering power P_s and the double-bounce scattering power P_d become zero because the sum of P_v and P_c should not exceed the total power.

3) $P_s < 0$ or $P_d < 0$: The cause for negative powers comes from setting either $\alpha = 0$ or $\beta = 0$ to determine surface scattering or double-bounce scattering, although the occurrence is very rare. For example, once surface scattering is found to be dominant, we set $\alpha = 0$, and determine the main contribution P_s. After that, we calculate out P_d. This final value of P_d happens to be negative in anomalous points. Because the negative values appear in spiky noise fashion as shown in Fig. 2(b), we impose the total power constraints that all powers should be less than the total power so that

$$\text{If } P_s < 0, \text{then } P_s = 0 \text{ and } P_d = \text{TP} - P_v - P_c$$
$$\text{If } P_d < 0, \text{then } P_d = 0 \text{ and } P_s = \text{TP} - P_v - P_c.$$

This enforcement does not cause erroneous decomposition result at all as seen in Fig. 2(c).

C. Modified Decomposition Algorithm

Fig. 3 shows the modified algorithm for the four-component scattering power decomposition. The modification from the previous one [2] is the power constraint that all the decomposed powers should be greater than zero and less than the total power (span).

Fig. 2(c) shows the color-coded composite image of decomposition results with red (P_d), green (P_v), blue (P_s), and pink (P_c), respectively. The decomposed image seems quite satisfactory in comparison with Fig. 2(a). In addition, the transect profile after the modification is shown in Fig. 2(d), where all powers are positive.

TABLE I
Pi-SAR DATA SPECIFICATIONS

Date	Incidence angle (deg.)	
2004/ 2/ 4	31.71 – 46.13	
2004/ 8/ 4	30.19 – 44.18	
2004/11/ 3	31.19 – 45.49	
Frequency	L-band	X-band
Pixel size (m^2)	2.5 by 2.5	1.25 by 1.25
Averaging size (pixels)	5 by 5	10 by 10

(a) Aerial photo of *SAKATA*

(b) Lotus

(c) Reeds

Fig. 4. Sakata, Niigata, Japan. (a) Aerial photo of Sakata. (b) Lotus. (c) Reeds.

IV. Pi-SAR OBSERVATIONS

We applied the modified scheme to high-resolution data sets acquired with the Pi-SAR over a wet land. The Pi-SAR is an airborne POLSAR system developed by the National Institute of Information and Communications Technology (NICT) (X-band) and the Japan Aerospace Exploration Agency (JAXA) (L-band), Japan. It operates at two frequency (L and X) bands. The resolution on the ground is 1.5 × 1.5 m in the X-band and 3 × 3 m in the L-band. The specifications are listed in Table I.

The area under study is a small lagoon, Sakata in Niigata Prefecture, Japan. Fig. 4 shows the aerial photo. In the middle of the lagoon, lotus grows in summer. The rim is surrounded by reeds. The water level changes from season to season. This area has been registered with the Ramsar Treaty on Wetlands of International Importance particularly as a migratory waterfowl habitat for migrating birds. It is highly important to investigate the seasonal environment of these preserved areas to develop international POLSAR image assessment algorithms for global wetland monitoring.

V. POLSAR DATA ANALYSIS FOR ENVIRONMENTAL CHANGE

The modified four-component decomposition scheme was applied to the POLSAR image data sets acquired by the Pi-SAR sensor.

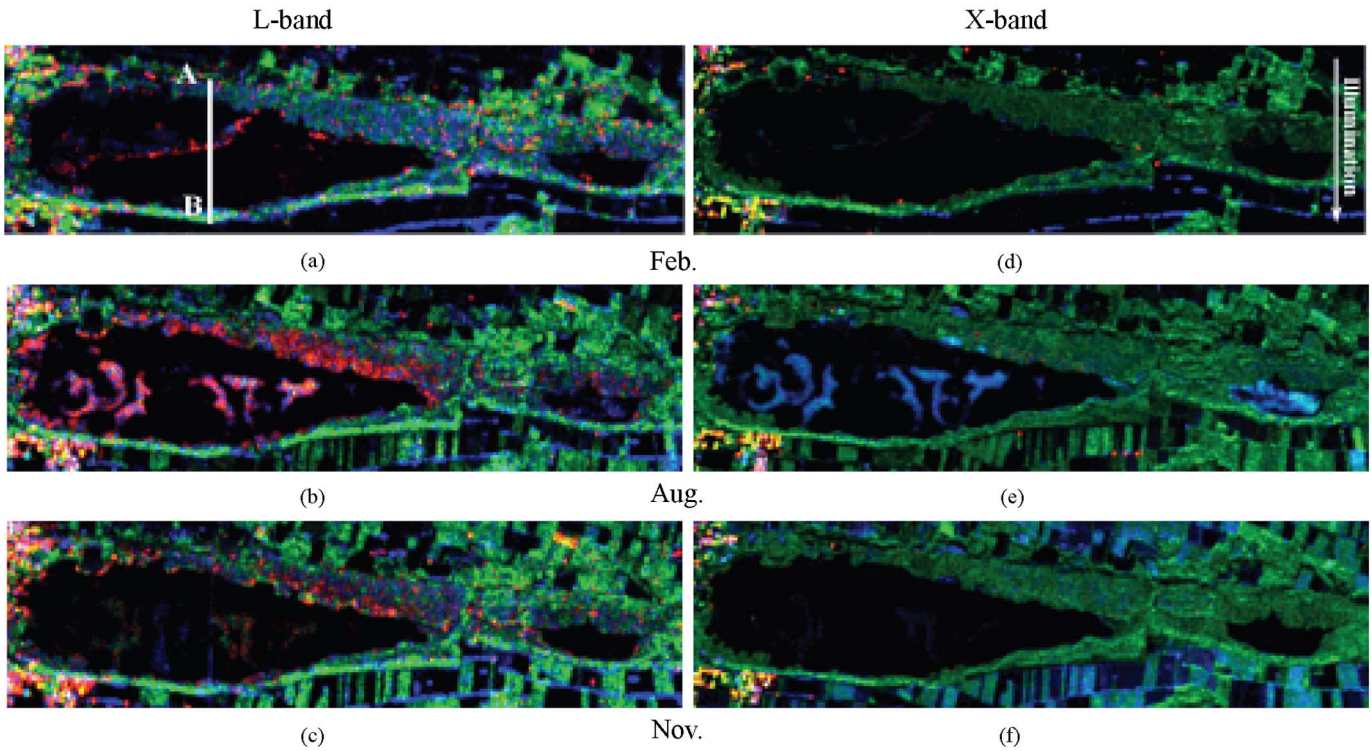

Fig. 5. Color-coded composite image of decomposed powers of Sakata area: (a)–(c) L-band, (d)–(f) X-band.

The size of the processing window or the number of ensemble averages is an important factor for accurate decomposition. If the number is too large, resolution of the decomposed image is lost, and the scattering characteristics are merged together. On the other hand, if the number is too small, the averaged quantities do not obey the theoretical second-order statistics. In this paper, the window size was chosen to be 10×10 pixels in the X-band data, and 5×5 pixels in the L-band data so that the resolution on the ground become the same (15×15 m). The window size is determined after the examination of convergence of the second-order statistics together with the resolution.

Fig. 5 shows the color-coded composite images of the decomposed results of both L- and X-band polarimetric data. The scattering powers are color coded as green for P_v (volume scattering), red for P_d (double-bounce scattering), and blue for P_s (surface scattering), respectively. Because P_c was small enough compared to other powers, it was omitted for illustration.

As Fig. 5 shows, there are pronounced changes in the scattering mechanisms. Both the L- and X-band images are dark in February [Fig. 5(a) and (d)] because the area is covered with snow, and snow cover acts like an electromagnetic absorber. The bright red and yellow areas in the left corner of the decomposed image are caused by houses [see Fig. 4(a)].

In the middle of summer, the vegetation cover is rich, causing P_s and P_d to be larger. Of special interest is the middle of the lake. The L-band image yielded red (P_d), while the X-band image produced blue (P_s). The reason for the difference is the scattering mechanism in the frequency band within the lotus and the reed beds. The vertical stems of the reeds and the water surface constitute a right-angle structure on the water surface, causing double-bounce scattering in the L-band. On the other hand, the vegetation structures cannot act as a corner reflector for the X-band because of the shorter wavelength and the attenuation within the structures. The X-band wave cannot penetrate deeply through the vegetation canopy.

In addition, the P_s (blue) in the lagoon in the X-band image [Fig. 5(e)] is caused only by the lotus in August. Because the lotus has thick broad leaves, the surface scattering dominates in the X-band. In November, some crops are harvested, and some are ripening. This situation caused various diverse patterns nearby the lake in the L- and X-band images. The blue color (P_s) is caused by rough surface scattering in the crop field after harvesting.

To examine the image analysis quantitatively, we looked at a transect, as indicated in Fig. 5(a). This transect included reeds on a water boundary, ice in winter, lotus, water, and soil; therefore, seasonal variation can be recognized. We calculated the values of the decomposed powers along the transect, resulting in Fig. 6. It reflects the status of each of the scattering mechanisms in the L-band.

From inspection of Fig. 6, we see that P_d agrees with the growing stage of reeds. There is no P_d in February because P_d increases in summer and decreases in November. In August, the contributions of P_s and P_d are almost the same for the lotus. The contribution of P_s and P_d may be used to monitor the status of bushes, reeds, and shrubs around the wetland area. It is possible to see the seasonal changes as well as the status of each scattering type by L-band Pi-SAR data.

Finally, an overlay image of the decomposed powers in the L-band (August) and the aerial photo in Fig. 4(a) are

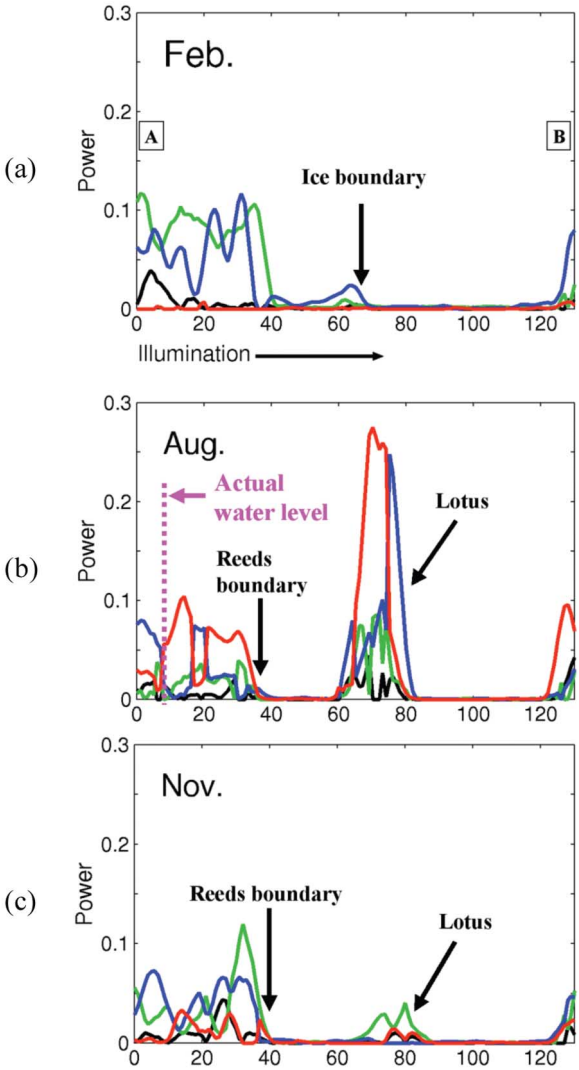

Fig. 6. Contribution of L-band three scattering powers along transect in Fig. 5. (a) February, (b) August, (c) November.

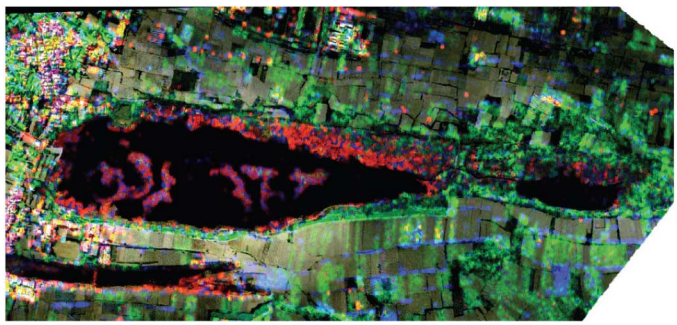

Fig. 7. L-band overlay image on Fig. 4(a).

shown in Fig. 7. A perfect match can be observed in this figure, indicating that the modified decomposition scheme is effective.

VI. Concluding Remarks

A modified four-component scattering power decomposition scheme was proposed for retrieving scattering characteristics of polarimetric SAR images. Then the new polarimetric decomposition scheme is applied to monitor seasonal changes of wetland areas. We found that the decomposed images clearly exhibit seasonal changes of the wetland area. From the decomposed results, it is possible to extract for wetland: water area (P_s) in wetland, which is related to water volume estimation; and growing stage of vegetation (through P_s and P_d).

Beause POLSAR systems such as ALOS-PALSAR (January 24, 2006), TerraSAR-X (June 15, 2007), and RadarSAT-2 (December 14, 2007) will all have polarimetric observation modes, their data will provide a powerful tool for monitoring the wetland environment such as those listed under the Ramsar Treaty, as well as those not yet included but are of similar importance.

Appendix
Criterion (12)

This criterion (12) is based on the equations of (21d) and (23) in [3]. Because the sign of $\mathrm{Re}\langle S_{HH}S_{VV}^*\rangle$ and the contained information are easily examined by the covariance matrix approach, we write one of the expansions of the covariance matrix decomposition.

$$\langle S_{HH}S_{VV}^*\rangle = f_s\beta + f_d\alpha + \frac{2}{15}f_v - \frac{f_c}{4}. \qquad \text{(21d) in [3]}$$

The expansion coefficients $f_v(=P_v)$ and $f_c(=P_c)$ are in the same notation as in [3]. It is seen that all scattering coefficients (f_s, f_d, f_v, and f_c) are connected to $\langle S_{HH}S_{VV}^*\rangle$. By using

$$f_v = \frac{15}{2}\left(\langle|S_{HV}|^2\rangle - \frac{f_c}{4}\right) \qquad \text{(23) in [3]}$$

we obtain the following form:

$$f_s\beta + f_d\alpha = C_0 = \langle S_{HH}S_{VV}^*\rangle - \langle|S_{HV}|^2\rangle + \frac{1}{2}P_c. \qquad (12)$$

The left-hand side of (12) consists of the surface and the double-bounce scattering terms only. In other words, the effect of the volume scattering and the helix scattering terms are subtracted in C_0. Therefore, the sign of C_0 is more precise for distinguishing both scattering terms rather than the sign of (21d).

Acknowledgment

The authors are grateful to the Pi-SAR operating teams of NICT and JAXA for providing Pi-SAR data sets.

References

[1] A. Freeman and S. L. Durden, "A three-component scattering model for polarimetric SAR data," *IEEE Trans. Geosci. Remote Sens.*, vol. 36, no. 3, pp. 936–973, May 1998.
[2] Y. Yamaguchi, Y. Yajima, and H. Yamada, "A four-component decomposition of POLSAR images based on the coherency matrix," *IEEE Geosci. Remote Sens. Lett.*, vol. 3, no. 3, pp. 292–296, Jul. 2006.
[3] Y. Yamaguchi, T. Moriyama, M. Ishido, and H. Yamada, "Four-component scattering model for polarimetric SAR image decomposition," *IEEE Trans. Geosci. Remote Sens.*, vol. 43, no. 8, pp. 1699–1706, Aug. 2005.
[4] J. S. Lee, M. R. Grunes, E. Pottier, and L. F. Famil, "Unsupervised terrain classifcation preserving polarimetric scattering characteristics," *IEEE Trans. Geosci. Remote Sens.*, vol. 42, no. 4, pp. 722–731, Apr. 2004.

[5] Y. Yamaguchi, Y. Yajima, R. Sato, H. Yamada, and W.-M. Boerner, "Decomposition of POLSAR image applied to wet land monitoring," in *Proc. ISAP*, Singapore, Nov. 2006.
[6] Ramsar Treaty. [Online]. Available: http://www.ramsar.org/
[7] J. S. Lee, D. Schuler, T. L. Ainsworth, E. Krogager, D. Kasilingam, and W. M. Boerner, "On the estimation of radar polarization orientation shifts induced by terrain slopes," *IEEE Trans. Geosci. Remote Sens.*, vol. 40, no. 1, pp. 30–41, Jan. 2002.

Yuki Yajima received the B.E. and M.E. degrees in information engineering from Niigata University, Niigata, Japan, in 2005 and 2007, respectively.

He was a graduate student at Niigata University where he had been engaged in POLSAR image analysis.

Yoshio Yamaguchi (M'83–SM'94–F'02) received the B.E. degree in electronics engineering from Niigata University, Niigata, Japan, in 1976, and the M.E. and Dr. Eng. degrees from the Tokyo Institute of Technology, Tokyo, Japan, in 1978 and 1983, respectively.

In 1978, he joined the Faculty of Engineering, Niigata University, where he is a Professor. From 1988 to 1989, he was a Research Associate at the University of Illinois at Chicago. His interests are in the field of radar polarimetry, microwave sensing, and imaging.

Dr. Yamaguchi was Chair of the IEEE Geoscience and Remote Sensing Society Japan Chapter (2002–2003), Vice Chair (2000–2001), organizer of Polarimetric-SyntheticAperture Radar Workshops (2000–2005) in Japan, and Associate Editor for Asian affairs of the *GRSS Newsletter* since 2003. He is a Fellow of the Institute of Electronics, Information and Communication Engineers, Japan, and the Electromagnetics Academy.

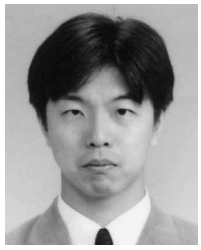

Ryoichi Sato (M'04) received the B.S., M.S., and Ph.D. degrees in electrical engineering from Chuo University, Tokyo, Japan, in 1992, 1994, and 1997, respectively.

Since April 1997, he has been with the Faculty of Education and Human Sciences, Niigata University, Niigata, Japan, where he is currently an Associate Professor. In 2002, he was a Research Scholar at Polytechnic University, Brooklyn, NY. His current research interests are in electromagnetic wave propagation.

Hiroyoshi Yamada (M'93) received the B.E., M.E., and Dr. Eng. degrees from Hokkaido University, Sapporo, Japan, in 1988, 1990, and 1993, respectively, all in electronic engineering.

In 1993, he joined the Faculty of Engineering, Niigata University, Niigata, Japan, where he is an Associate Professor. From 2000 to 2001, he was a Visiting Scientist at the Jet Propulsion Laboratory, California Institute of Technology, Pasadena. His research interests are in the field of array signal processing, polarimetric radar interferometry, and high-resolution techniques.

Dr. Yamada is a member of the Institute of Electronics, Information and Communication Engineers of Japan.

Wolfgang-Martin Boerner (SM'75–F'84–LF'92) received the Ph.D. degree from the University of Pennsylvania, Philadelphia, in 1967.

From 1967 to 1968, he was with the University of Michigan, Ann Arbor. In 1968, he was with the University of Manitoba, Winnipeg, Canada. Since 1978, he has been a Professor in the Department of Electrical and Computer Engineering at the University of Illinois at Chicago. His research interests are electromagnetic vector inverse scattering, radar polarimetry, polarimetric interferometry, and tomography.

Dr. Boerner is a Senior Member of CAP, American Society of Engineering Education, American Society for Remote Sensing and Photogrammetry, International Society for Remote Sensing and Photogrammetry, Optical Society of America, International Society for Optical Engineering, American Association for the Advancement of Science, and Institute of Electronics, Information and Communication Engineers. He is a member of the Sigma Xi honor society, the American and the German Fulbright Associations, and the Alexander von Humboldt Association.